2020

Validated model of platelet slip at stenosis and device surfaces

Denardo, Scott J.; Denardo, Bruce C.; Carpinone, Paul L.; Dean, William T.; New, David M.; Estrada, Luis E.; Green, Cynthia L.; Yock, Paul G.; Karunasiri, Gamani

Taylor & Francis

Scott J. Denardo, Bruce C. Denardo, Paul L. Carpinone, William T. Dean, David M. New, Luis E. Estrada, Cynthia L. Green, Paul G. Yock & Gamani Karunasiri (2020) Validated model of platelet slip at stenosis and device surfaces, Platelets, 31:3, 373-382

http://hdl.handle.net/10945/65256

http://www.tandfonline.com/iplt
ISSN: 0953-7104 (print), 1369-1635 (electronic)

platelets

Platelets, 2020; 31(3): 373–382
 DOI: https://doi.org/10.1080/09537104.2019.1636021

Taylor & Francis
Taylor & Francis Group

Check for updates

Validated model of platelet slip at stenosis and device surfaces

Scott J. Denardo[1], Bruce C. Denardo[2], Paul L. Carpinone[3], William T. Dean[2], David M. New[2], Luis E. Estrada[2], Cynthia L. Green[4], Paul G. Yock[5], & Gamani Karunasiri[2]

[1]Reid Heart Center/FirstHealth of Carolinas Cardiac and Vascular Institute, Pinehurst, NC, USA, [2]Department of Physics, Naval Postgraduate School, Monterey, CA, USA, [3]Particle Engineering Research Center, University of Florida, Gainesville, FL, USA, [4]Department of Biostatistics and Bioinformatics, Duke University Medical Center, Durham, NC, USA, and [5]Department of Bioengineering, Stanford University, Stanford, CA, USA.

Abstract

Platelets are central to thrombosis. However, it is unknown whether platelets slip at vascular or device surfaces. The presence of platelet slip at a surface would interrupt physical contact between the platelet and that surface, and therefore diminish adhesion and thrombosis. Unfortunately, no existing technology can directly measure platelet slip in a biological environment. The objective of this study was to explore whether microspheres–modeling platelets–slip at different vascular and device surfaces in an acrylic scaled-up model coronary artery. The microspheres (3.12 μm diameter) were suspended in a transparent glycerol/water experimental fluid, which flowed continuously at Reynolds numbers typical of coronary flow (200–400) through the model artery. We placed a series of axisymmetric acrylic stenoses (cross-sectional area reduction [CSAr], 20–90%) into the model artery, both without and with a central cylinder present (modeling a percutaneous interventional guide wire, and with a scaled-up Doppler catheter mounted upstream). We used laser Doppler velocimetry (LDV) to measure microsphere velocities within, proximal and distal to each stenosis, and compared to computer simulations of fluid flow with no-slip. For validation, we replaced the acrylic with paraffin stenoses (more biologically relevant from a surface roughness perspective) and then analyzed the signal recorded by the scaled-up Doppler catheter. Using the LDV, we identified progressive microsphere slip proportional to CSAr inside entrances for stenoses ≥60% and ≥40% without and with cylinder present, respectively. Additionally, microsphere slip occurred universally along the cylinder surface. Computer simulations indicated increased fluid shear rates (velocity gradients) at these particular locations, and logistic regression analysis comparing microsphere slip with fluid shear rate resulted in a c-index of 0.989 at a cut-point fluid shear rate of (10.61 [cm^{-1}]×mean velocity [cm×sec^{-1}]). Moreover, the presence of the cylinder caused disordering of microsphere shear rates distal to higher grade stenoses, indicating a disturbance in their flow. Finally, despite lower precision, the signal recorded by the scaled-up Doppler catheter nonetheless indicated slip at the entry into and at most locations distal to the 90% stenosis. Our validated model establishes proof of concept for platelet slip, and platelet slip explains several important basic and clinical observations. If technological advances allow confirmation in a true biologic environment, then our results will likely influence the development of shear-dependent antiplatelet drugs. Also, adding shear rate information, our results provide a direct experimental fluid dynamic foundation for antiplatelet-focused antithrombotic therapy during coronary interventions directed towards higher grade atherosclerotic stenoses.

Keywords

Cardiovascular, hydrodynamics, models, platelet adhesiveness, shear strength, thrombosis

History

HistoryReceived 5 March 2018
Revised 8 June 2019
Accepted 8 June 2019
Published online 13 July 2019

Introduction

In fluid dynamics, slip at any fluid-solid interface indicates that the fluid has a non-zero velocity at the surface of the solid (Figure 1, left panel) [1]. For macroscopic Newtonian fluid flow (e.g. water and glycerol), there is no appreciable slip at solid surfaces, resulting in the "no-slip" boundary condition [2]. Thus, there is an infinitesimally thin layer of fluid at the surface that is not moving. However, mathematical models [3,4] and experimental data involving concentrated suspensions [5,6] indicate small particles contained within a Newtonian fluid can slip.

Blood has been modeled as both a Newtonian and a non-Newtonian fluid [7]. However, it is in fact non-Newtonian and thus capable of slip [2,8]. Blood is composed of cells and platelets suspended in plasma. On a microscopic scale, red blood cells and plasma demonstrate true and apparent slip at solid surfaces, respectively (Figure 1, right panel) [9,10]. Platelets are central to thrombosis [11], and they may "roll" along a site of vascular injury [12]. However, it is unknown whether platelets slip [13]. The presence of platelet slip at a surface would interrupt physical contact between the platelet and that surface. Thus, platelet slip would diminish adhesion and therefore thrombosis at that surface [11,14], which would have

Color versions of one or more of the figures in the article can be found online at www.tandfonline.com/iplt.

Research Site: Department of Mechanical Engineering, University of California, Berkeley; Berkeley, CA, USA.

Correspondence: Scott J. Denardo and MD Reid Heart Center/FirstHealth of Carolinas Cardiac and Vascular Institute, 155 Memorial Drive, Pinehurst, NC 28374, USA. Phone: 910.416.9037 Fax: 910.571.5539. E-mail: scott.denardo@duke.edu

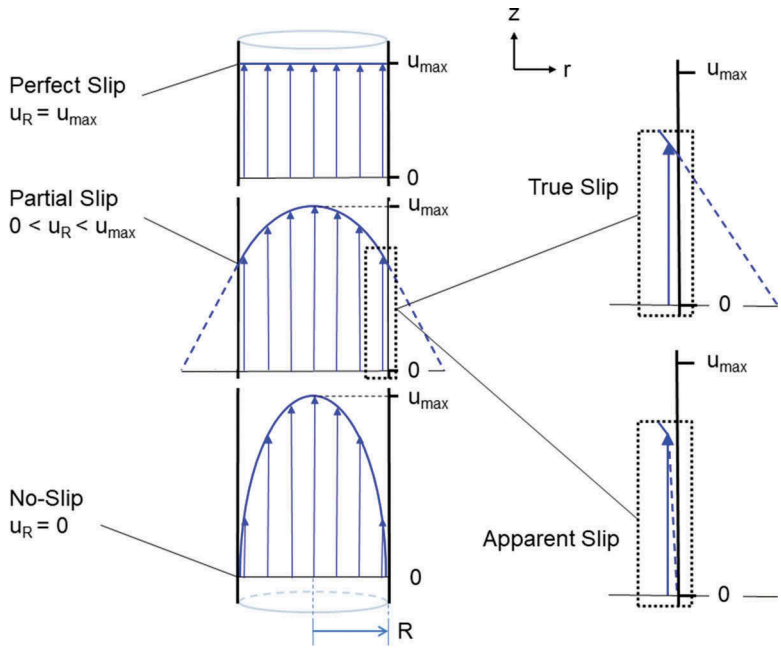

Figure 1. Velocity profile of fluid flow through a cylinder. Lower left panel: no-slip boundary condition. Middle left panel: partial slip. Upper left panel: perfect slip. True slip (upper right panel) indicates the slip layer at the boundary is of molecular dimension, and apparent slip (lower right panel) indicates the local velocity varies over a finite, albeit small, mesoscopic distance [4]. Fluid flow is in the z-direction, steady, laminar and incompressible. R = cylinder inside radius; u_R = fluid velocity at cylinder inside surface ("slip velocity"); u_{max} = maximum flow velocity.

important implications for thrombosis in both normal and diseased vascular systems, as well as at device surfaces.

There is no technology currently available to directly measure platelet slip in a biological environment. In this study, we use laser Doppler velocimetry (LDV) and conventional Doppler ultrasound to explore whether microspheres–modeling platelets–slip at different vascular and device surfaces in a scaled-up model coronary artery, with different flow conditions representing common *in vivo* situations. We then apply our results to explain several important basic and clinical cardiovascular observations involving platelets.

Materials and Methods

Scaled-up Model Coronary Artery

Our scaled-up model coronary artery and flow system have been described (Figure 2a) [15]. The data collection period for this project was from July, 1989, through February, 1990. The experimental fluid was a transparent mixture of distilled water and glycerol, which is commonly used to simulate blood [16]. The fluid was seeded with 3.12 μm diameter polystyrene microspheres (Duke Scientific Industries; Palo Alto, CA, USA) at a relatively dilute concentration of 2.5×10^4 particles×ml^{-1}. Rigid microspheres have been shown to behave fluid dynamically similar to platelets [17], but with interactions (e.g. van der Waals) confined to a range of ≤20 nm [18]. Our microspheres therefore modeled platelets and simultaneously provided a signal for both the LDV and conventional Doppler ultrasound [15,17], without discernably promoting slip. The composite fluid was Newtonian (Figure 2a, inset), and therefore also did not promote slip. The fluid flowed continuously through an acrylic, cylindrical test section (inside diameter [D], 25.4 mm), which modeled a coronary artery. A flowmeter adjusted the Reynolds numbers (RE) to be representative of coronary blood flow (range, 200–400 ± 5%) [19].

Axisymmetric stenoses were lathed from acrylic rods (transparent, but ultrasound-reflective) and paraffin blocks (opaque, but ultrasound-absorptive) followed by high-frequency polishing. Their specifications were: outside length, 2D; entrance and exit angles, 45°; cross-sectional area reduction (CSAr) 20%, 40%, 60%, 75% and 90%. A stainless-steel cylinder (outside diameter, 0.20D) was also placed centrally into the model (Figure 2a), representing a guide wire used during coronary interventions. It was painted flat black (non-superhydrophobic) to reduce any reflective interference on LDV measurements. A scaled-up Doppler catheter was mounted upstream on this central cylinder.

Optical microscopy (Olympus BX 60; Olympus America Incorporated; Center Valley, PA, USA) of the different surfaces in the model revealed very different appearances (Figure 2b). However, each acrylic surface and the surface of the central cylinder demonstrated a contact angle <90°-indicating hydrophilicity-and therefore not intrinsically promoting slip [2]. Moreover, the paraffin stenosis surfaces demonstrated a contact angle of 110°-indicating hydrophobicity-and therefore potentially promoting slip. Profilometry (Zygo NewView 5000; Zygo Corporation; Middlefield, CT, USA) showed that all acrylic surfaces were uniformly smoother compared with paraffin surfaces (Figure 2b; maximum $p < 0.001$). Also, for both acrylic and paraffin stenoses, surface roughness did not statistically correlate with CSAr ($r = -0.065$, $p = 0.672$; $r = -0.015$, $p = 0.889$; respectively). From a contact angle perspective, the acrylic and paraffin stenoses spanned endothelium [20]. Additionally, the length scale of the surface roughness of the paraffin stenoses closely modeled endothelium [21].

Experimental Measurement and Analysis of Microsphere Velocities: LDV

The LDV (wavelength, 514 nm; sample volume dimensions, 0.320 mm(0.0126D)-radial×0.160 mm(0.0063D)-axial ×0.160 mm(0.0063D)-azimuthal) [15] was positioned transverse to the axis of flow (Figure 2a). It measured microsphere velocities from the horizontal middle plane at discrete axial and radial locations, both before and after central placement of the cylinder (and scaled-up Doppler catheter). LDV measurements were made at nine axial locations relative to each acrylic stenosis (three within, two proximal, four distal). The velocity data were collected starting with the center of the LDV sample volume at 1.00 mm inside each stenosis (or test section) surface, and then at 1.00 mm radial increments towards the centerline (or central cylinder surface). However, inside the 75% and 90% stenoses, data were collected at 0.50 mm and 0.25 mm increments, respectively. No LDV data were acquired with the sample volume center ≤0.160 mm from a surface due to lateral migration of microspheres [17] and potential LDV measurement error [15,22]. As

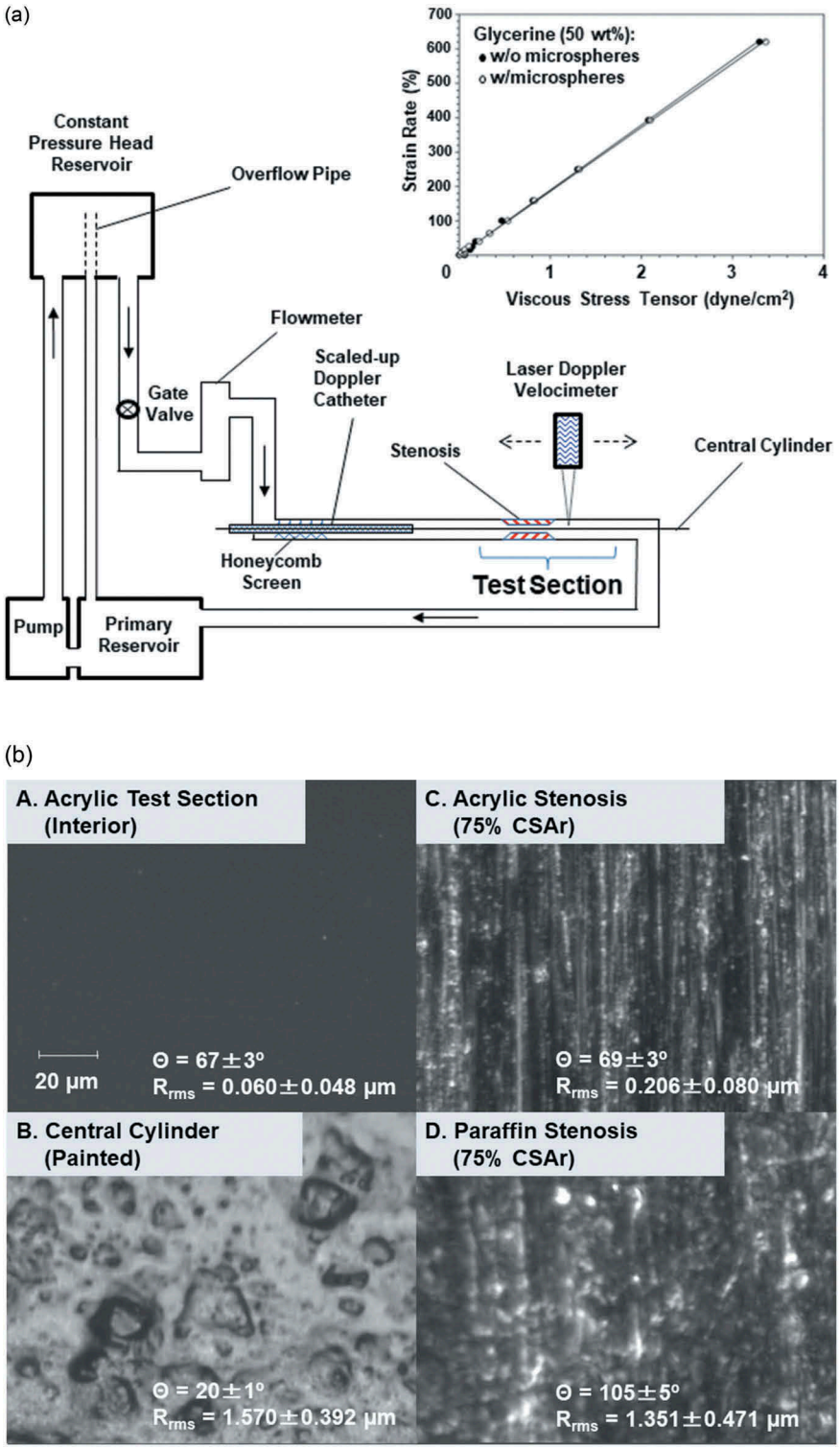

Figure 2. (a) Schematic diagram of scaled-up model coronary artery and flow system. The stenoses were placed individually into the cylindrical test section 55D downstream from the honeycomb screen to ensure delivery of fully developed, non-swirling laminar flow. A scaled-up Doppler catheter-with dimensions similar to a stent delivery system-was mounted upstream on the central cylinder. Inset: The linear relationship between strain rate vs. viscous stress of the experimental fluid indicates Newtonian behavior, both without and with polystyrene microspheres present. D = test section inside diameter (25.4 mm). (b) Optical micrographs, contact angles (Θ) and surface roughness (R; root mean square–rms) of the different surfaces in the model. The direction of fluid flow is from left-to-right. Θ ≤ 90° indicates hydrophilic surface; Θ > 90° indicates hydrophobic surface [2]. For comparison, rabbit aorta endothelium Θ = 86°; rabbit aorta subendothelium Θ = 20° [20]; and porcine coronary artery endothelium R = 0.90–1.27 μm (distal-to-proximal) [21]. Data are presented as mean±SD, and for stenoses represent aggregate data over all 5 CSAr. SD = standard deviation; CSAr = cross-sectional area reduction.

a consequence of this restriction and with the geometry of our model, the distance from the final LDV sample volume center to the central cylinder surface was 0.161 mm for LDV measurements immediately adjacent to the central cylinder surface proximal and distal to all stenoses (30/45 = 67% of all LDV measurements adjacent to the cylinder). Within stenoses (remaining 15/45 = 33% of LDV measurements adjacent to cylinder), the median distance from the LDV sample volume center to the central cylinder surface was 0.310 mm [(25th, 75th percentiles): (0.297, 0.492 mm)].

LDV data were compared with computer simulations of fluid flow with no-slip. Slip velocities and shear rates (velocity gradients) of microspheres at each surface were interpolated from the final two LDV data points adjacent to the surface [16].

Experimental Measurement and Analysis of Microsphere Velocities: Conventional Doppler Ultrasound

To acquire an independent experimental measurement of microsphere velocities using an alternate measurement technique in a somewhat more biologically relevant model (from a surface roughness perspective), we recorded mean velocity data at the nine prespecified axial locations using conventional Doppler ultrasound produced by the scaled-up Doppler catheter (OD, 0.50D; frequency,

5.0 MHz) (Figure 2a) [15], and we replaced the acrylic stenoses with the paraffin stenoses. Notably, the diameter and profile of the scaled-up Doppler catheter also modeled a typical stent delivery system. The range gate distance for the scaled-up Doppler catheter was set at ≥3.0D, and therefore ≥1.6D beyond the flow disturbance created by the step-down at its distal end [23]. The sample volume axial length was 3.93 mm (0.155D)-modeling a contemporary Doppler catheter for human use-and a stack of paraffin discs (OD, 0.89D) was placed on the distal cylinder to prevent multiple sample volumes [15]. As a consequence of the axial length of the scaled-up Doppler catheter sample volume compared with the axial length of the LDV sample volume (0.155D/0.0063D = 24.6), the precision of the scaled-up Doppler catheter was much less compared with LDV.

The electronic signal recorded by the scaled-up Doppler catheter was processed using a fast Fourier transform, and produced a mean velocity with standard deviation (SD). However, the distribution of beam power produced by the catheter was not homogeneous [15]. Thus, the mean velocity reported by the catheter was the summed spatial average of local fluid velocity weighted by local beam power within the sample volume [15]. Consequently, to predict the mean velocity produced by the scaled-up Doppler catheter, the microsphere velocities recorded by LDV were weighted by the beam power distribution. Following this correction for inhomogeneous beam power distribution and accounting for amplified beam expansion distal to the higher grade stenoses [15,24], we compared the mean velocity predicted by the LDV microsphere velocities with the mean velocity recorded by the scaled-up Doppler catheter. Finally, we compared the mean velocity using computer simulations (with imposed no-slip condition) after correction for the inhomogeneous beam power distribution with the same mean velocity recorded by the scaled-up Doppler catheter.

Computer Simulation

To simulate fluid flow, we used the COMSOL Multiphysics software (COMSOL, Inc.; Palo Alto, CA, USA). This software generates discrete velocity profiles and at default applies conventional fluid dynamic theory with no-slip at surfaces. The simulation environment was two dimensional, axisymmetric, and the reference was the radial center of the scaled-up model. The fluid parameters were laminar flow, Newtonian and incompressible. All surfaces were designated impermeable. Meshing within COMSOL was set to be normal (approximately 15 discrete elements across at the narrowest point) as more fine resolutions yielded no appreciable change for any experimental conditions.

The COMSOL stationary solver–which determines the nature of all parameters once a steady state has been achieved-was used to extract solutions for direct comparison with LDV measurements. At each pre-specified axial location, velocity profiles were recorded and exported from the COMSOL software package as a spreadsheet. The data were then graphed for comparison with LDV measurements.

Statistical Analysis

LDV data are presented using the mean and SD, normalized to mean velocity. Because of the discrete velocity profile generated by COMSOL, LDV microsphere velocities were considered significantly different only if their mean values differed by ≥2SD from COMSOL. A univariable logistic regression model for microsphere slip was applied to each variable of shear rate, surface roughness, CSAr and central cylinder presence, followed by a multivariable analysis. The final model was then used to determine the threshold at which fluid shear rate predicts slip by maximizing the area (c-index) under the receiver operating characteristics curve (ROC). Results are presented as odds ratio (OR) with 95% confidence interval (CI). A two-sample t-test was used to compare coefficients of variation (CV = SD/mean) in microsphere velocity at various locations of slip and no-slip, while correlation between surface roughness and CSAr was determined using the Spearman correlation coefficient. A c-index ≥0.80 indicates strong model performance, while a p-value <0.05 is considered statistically significant. Statistical analyses were done using SAS version 9.4 (SAS, Inc., Cary, NC). For data that were the result of a product of variables (e.g. the product of LDV-measured microsphere velocity and beam power distribution), standard propagation of error analysis was performed.

Data Availability Statement

All data generated or analyzed in this study are presented in this published article with the exception of the scaled-up Doppler catheter beam power distribution data, which can be viewed as beam power distribution plots in the supplementary information file.

Results

LDV Measurements: Central Cylinder Absent

LDV-derived microsphere velocity profiles inside stenoses demonstrated anticipated blunting [16] that was most pronounced within the entrance (axial location −0.475D), and the blunting was proportional to CSAr (Figure 3a, upper row). Importantly, for stenoses with CSAr ≥60% and comparing with COMSOL, LDV demonstrated slip of microspheres at the stenosis surface that was most pronounced within each entrance and then dissipated through the exit. The blunting of velocity profiles and observed slip were consistent over the study RE range (Figure 3b). Additionally, the magnitude of slip and its propagation downstream through each stenosis exit, quantified by slip velocity, were proportional to CSAr (Figure 4, upper left). As a result of slip, all microsphere shear rates within the stenosis entrances remained relatively low (Figure 4, upper right). However, microspheres were still subjected to the COMSOL-documented increased shear rate of the local fluid flow (Figure 3a, upper row). Towards the axial center of the stenoses, as microsphere slip velocities decreased, their shear rates increased proportional to CSAr, and then in general decreased back towards baseline at the stenosis exits (excepting the 90% stenosis). At all stenosis exits and further distal, the shear rate of microspheres was similar to the shear rate of the local fluid flow.

LDV Measurements: Central Cylinder Present

Similar to central cylinder absent, velocity profiles inside stenoses with the cylinder present demonstrated progressive blunting proportional to CSAr (Figure 3a, lower row). Also, for stenoses with CSAr ≥40%, LDV showed slip at the stenosis surface that was most pronounced within each entrance. The slip was consistent over the study RE (Figure 3b), and the magnitude of slip was proportional to CSAr (Figure 4, middle left). However, in contrast to cylinder absent (solely excepting the 90% stenosis), slip had significantly dissipated by the axial center of each stenosis. Microsphere shear rates within the stenosis entrances remained relatively low (Figure 4, middle right), then increased to peak values distal within each stenosis (towards the exit) and finally returned to baseline just beyond the exit of each stenosis, similar to the shear rate of the local fluid flow.

COMSOL showed the change in fluid velocity profile caused by the central cylinder surface with no-slip (Figure 3a,b). This change resulted in a significant fluid shear rate at the surface of the cylinder. For example, at axial location −1.500D–where even the higher grade stenoses had only a very limited effect on the velocity profile at that

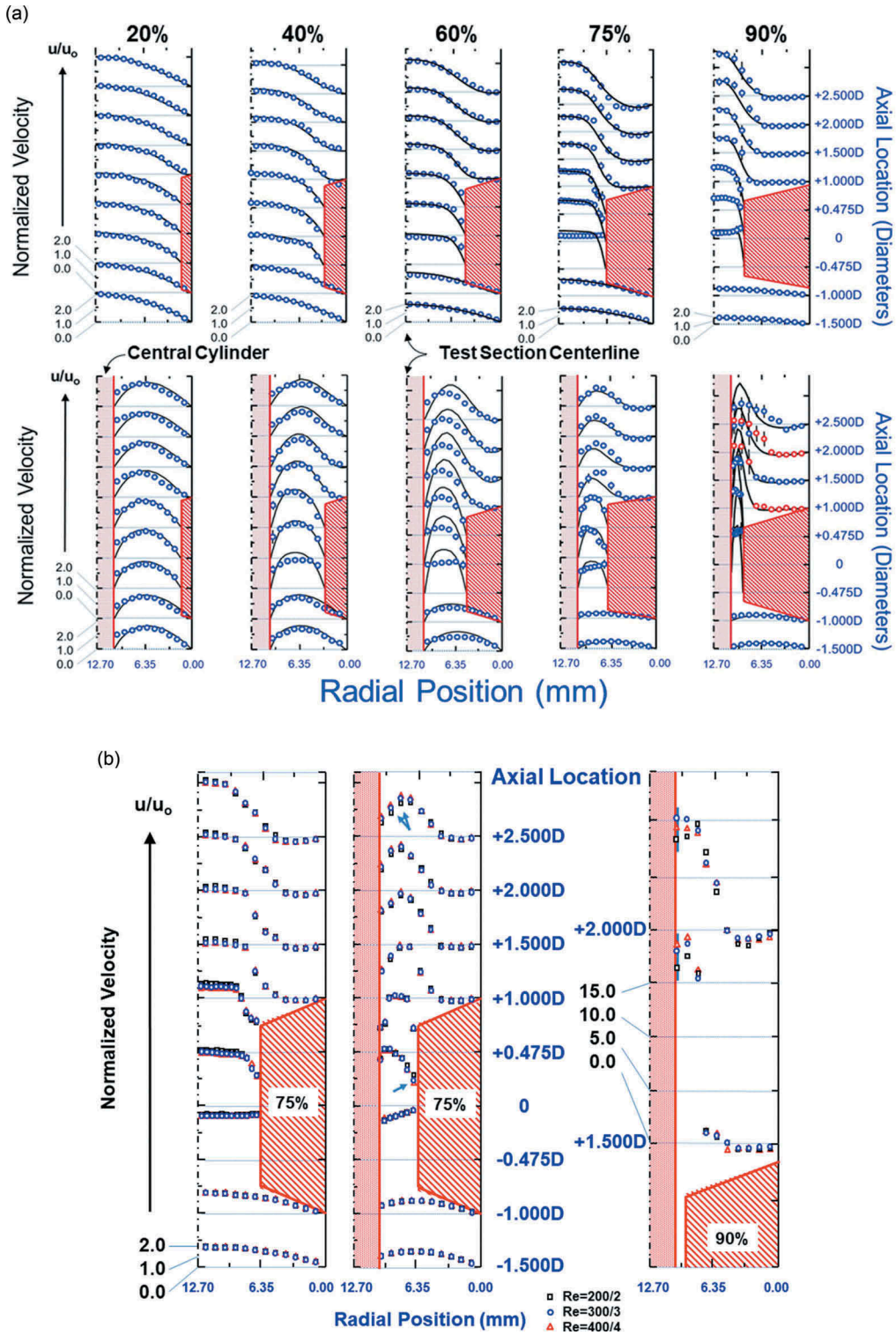

Figure 3. (a) Microsphere velocities determined by LDV (blue rings) compared with COMSOL computer simulated fluid velocity profiles (black solid lines) for RE 300. All velocities are normalized to the mean velocity calculated from direct volumetric measurement. Computer simulations apply the no-slip boundary condition at each surface. Upper row: central cylinder absent; Lower row: central cylinder present. The velocity scale shown for the velocity profile at axial location −1.500D for each stenosis in the upper panel applies to all remaining velocity profiles for that stenosis with cylinder absent and present. Each individual microsphere velocity data point is the average of 1024 samples. Standard deviations for microsphere velocity data are shown as vertical lines through the center of the ring only if greater than the radius of that ring, and are equal to one-half the length of the line. The LDV data points suggesting negative microsphere shear rate at the entrances to the 90% stenosis surface (without cylinder) and 75% stenosis surface (with cylinder) differ by <1SD, and are thus considered not significantly different. LDV = laser Doppler velocimetry; RE = Reynolds number; D = test section inside diameter; SD = standard deviation. (b) Superimposed LDV microsphere velocity profiles for 75% and 90% CSAr stenosis at RE 200, 300 and 400, with normalization to RE 100. Left-hand panel: 75% stenosis, cylinder absent; Middle panel: 75% stenosis, cylinder present; Right-hand panel, 90% stenosis, cylinder present, focused on axial locations +1.500D and +2.000D. The only significant differences (>2SD) in normalized velocity occurred for the 75% stenosis with the cylinder present, between RE 200 and 400 and at axial locations 0 and +2.500D (see arrows). The greatest absolute differences in normalized velocities for the 90% stenosis occurred adjacent to the cylinder surface but were <2SD. Standard deviations for velocity data are shown only for these data, and are equal to one-half the length of the line. In general, SD are otherwise less than the largest dimension of each symbol. LDV = laser Doppler velocimetry; CSAr = cross-sectional area reduction; RE = Reynolds number; D = test section inside diameter; SD = standard deviation.

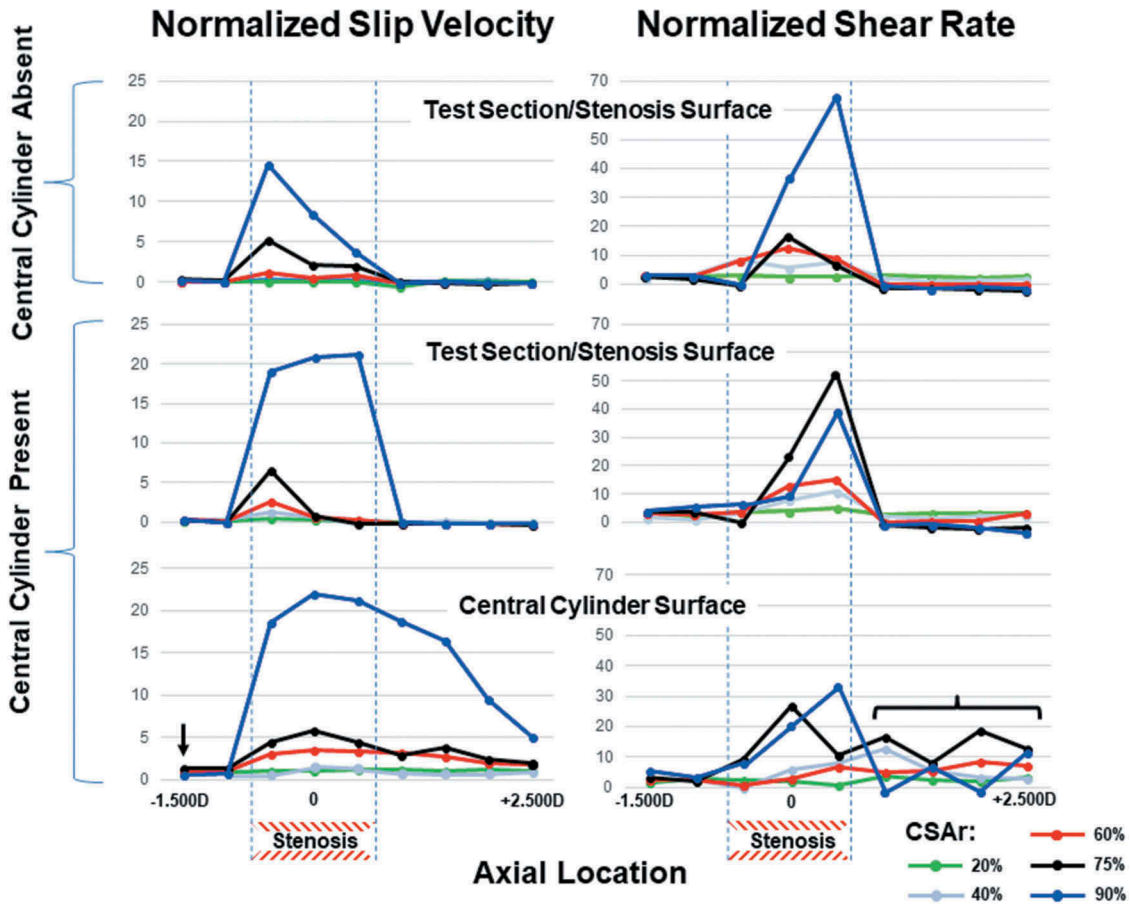

Figure 4. Microsphere slip velocity (left) and shear rate (right) normalized to mean velocity as a function of axial location and CSAr for RE 300. Top row: central cylinder absent. Middle and bottom rows: central cylinder present. The shear rates for the entrances to the 90% stenosis surface (without cylinder) and 75% stenosis surface (with cylinder) were set to zero, as the adjacent LDV data points contributing to the calculation differed by <1SD. The average normalized microsphere slip velocity at the central cylinder surface for axial location −1.500D (arrow, lower left panel) was 0.80 ± 0.21. Also, there was a disordering of shear rates of microspheres distal to the higher grade CSAr stenoses (horizontal bracket, lower right panel). CSAr = cross-sectional area reduction; RE = Reynolds number; LDV = laser Doppler velocimetry; SD = standard deviation; D = test section inside diameter.

proximal location [25]-the fluid shear rate was similar to the shear rate at the surface of the entrance (axial location −0.475D) into the 60% stenosis without cylinder (Figure 3a). Moreover, LDV showed microsphere slip universally along the cylinder surface (Figure 3a,b, 4-lower left). The normalized slip velocity at axial location −1.500D was on average [0.80 ± 0.21]×[mean velocity]. The slip velocity generally increased upon entry into each stenosis, and the increase was proportional to CSAr (Figure 4, lower left). Despite slip, microsphere shear rates also progressively increased at the cylinder surface down the length of each stenosis (Figure 4, lower right). Distal to each stenosis, the magnitude of slip decreased in general monotonically back towards the baseline value (at axial location −1.500D). However, in contrast to the fluid flow (Figure 3a), shear rates of microspheres became disordered distal to the higher CSAr stenoses (≥75%; Figure 4, lower right), indicating a disturbance in microsphere flow due to slip at the cylinder surface.

Additional Detailed Analysis of LDV Measurements and COMSOL Simulations

Additional detailed analysis comparing the LDV microsphere slip with COMSOL shear rates of fluid flow at all surfaces, normalized to mean velocity (in cm×sec^{-1}), showed that microsphere slip occurred at a critical normalized threshold fluid shear rate of 10.61 cm^{-1} (Figure 5). All slip occurred at-or-above this threshold, while a vast majority of no-slip occurred below. Logistic regression analysis using the critical threshold fluid shear rate as the cut-point maximized the area under the ROC curve (c-index = 0.989), with a sensitivity (Sn) and specificity (Sp) of 100% and 94%, respectively. Moreover, the univariable logistic regression models consisting of shear rate (OR = 1.54; 95%CI: 1.28–1.85; $p < 0.001$), surface roughness-per 0.10 increase (OR = 1.23; 95%CI: 1.12–1.35; $p < 0.001$), CSAr-per 10 increase (OR = 1.16; 95%CI: 1.01–1.34; $p = 0.036$) and central cylinder presence (OR = 6.0; 95%CI: 2.6–14.0; $p < 0.001$) also showed each was significantly predictive of slip (c-indexes = 0.989, 0.967, 0.601 and 0.679, respectively). However, only shear rate remained in the multivariable model.

To assess whether microsphere slip was a transient process or if the LDV failed to detect a developing local high microsphere velocity gradient at sites of reported slip due to insufficient measurement resolution, we compared the CV for velocities at the various locations of observed slip (e.g. adjacent to the surface at the entrance into and within intermediate-to-high grade stenoses, and along the surface of the central cylinder) with the CV for velocities at locations of no-slip and no other flow disturbance (specifically, adjacent to the test section surface at axial location −1.500). If microsphere slip was a transient process or if the LDV measurements failed to detect local high microsphere velocity gradients, then the CV would increase at sites of observed slip [15,26]. However, we found that the CV at locations of observed slip was less compared with locations of no-slip and no other flow disturbance (Table I). Thus, it appears that our observed

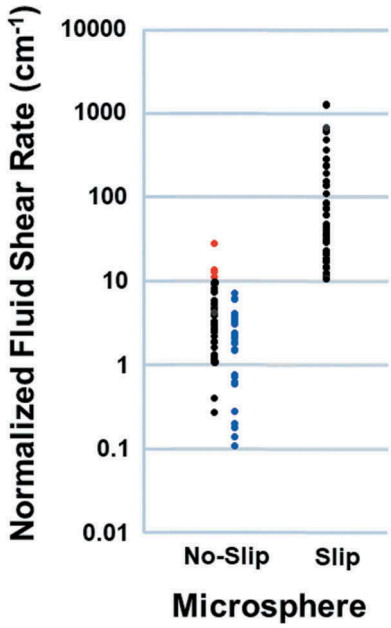

Figure 5. COMSOL-determined shear rate of fluid flow (normalized to mean velocity, u_0) at all surfaces as a function of microsphere no-slip vs. slip. Ordinate is in $\log_{10}$ scale. Data points in blue represent absolute values of normalized shear rates where the velocity of fluid flow was negative (i.e.: recirculation zones, downstream from stenoses). Microsphere slip occurred at a critical normalized threshold fluid shear rate of 10.61 cm^{-1}. The shear rates for the 4 no-slip data points in red were above the critical normalized threshold shear rate (range, 10.83–27.38 cm^{-1}), resulting in the only exceptions to mutual exclusivity. Importantly, 3/4 exceptions involved a decreasing shear rate as a function of axial location. Thus, on a more precise scale, slip may depend on higher order derivatives of shear rate as a function of location.

Table I. Average CV in microsphere velocity at locations of slip compared with the location of no-slip and no other flow disturbance (i.e.: axial location-1.500D, at test section surface).

Slip Condition/Location	CV (mean±SD)	P-value*
No-slip/ Test section surface	0.22±0.03	
Slip/ Stenosis surface	0.12±0.06	0.0005
Slip/ Central cylinder surface	0.13±0.05	0.0002

CV=coefficient of variation (microsphere velocity SD/mean); SD=standard deviation; D=test section diameter.
*Compared to reference group (no slip at test section surface).

microsphere slip was not a transient process and there were no local high microsphere velocity gradients that went undetected by the LDV.

Conventional Doppler Ultrasound Measurements Using Scaled-up Doppler Catheter

The mean velocity predicted by combining LDV-measured microsphere velocities and beam power distribution data was very close (on average [2.0 ± 6.9]% greater) to the mean velocity recorded by the scaled-up Doppler catheter (Figure 6). Additionally, at the entry into and at most locations distal to the 90% stenosis, combining LDV-measured microsphere velocities and beam power distribution data resulted in a more accurate predicted mean velocity compared with combining computer simulations (with their imposed no-slip condition) with the beam power distribution data (Figure 6).

Discussion

In this study, we used LDV and conventional Doppler ultrasound to experimentally demonstrate slip of microspheres at different vascular and device surfaces in a scaled-up model coronary artery, with different flow conditions representing common *in vivo* situations. The microspheres modeled platelets, and their slip was demonstrated by LDV most prominently at the surface of the entrance into intermediate-to-high grade stenoses and universally along the central cylinder surface. Importantly, the fluid was Newtonian and, considering the no-slip-promoting properties of all surfaces involving LDV measurements, the model did not intrinsically promote slip. To our knowledge, the experimental finding of slip of dilute particles in a macroscopic Newtonian fluid within a model promoting no-slip has never been recognized and formally reported. Moreover, this finding may be amplified for a denser suspension, such as platelets *in vivo* [5,6].

The scaled-up Doppler catheter analysis with the paraffin stenoses indicate microspheres slip in that more biologically relevant model (and consequently validated the LDV measurements). For example, within the entrance to the 90% stenosis, the LDV-measured microsphere velocities more accurately predicted the mean velocity recorded by the scaled-up Doppler catheter compared with COMSOL simulations (and imposed no-slip). The absence of this finding further downstream in this stenosis and the complete absence of this finding for the ≤75% stenoses was likely the result of the axial imprecision of the scaled-up Doppler catheter compared with LDV.

The scaled-up Doppler catheter recordings distal to the 90% stenosis were acoustically focused by that stenosis to the region immediately adjacent to the central cylinder, at least for axial locations in closer proximity to the stenosis exit [15,24]. Those recordings, similar to within the entrance to the 90% stenoses, were more accurately predicted using the LDV-measured microsphere velocities compared with computer simulations imposing no-slip, thus indicating slip.

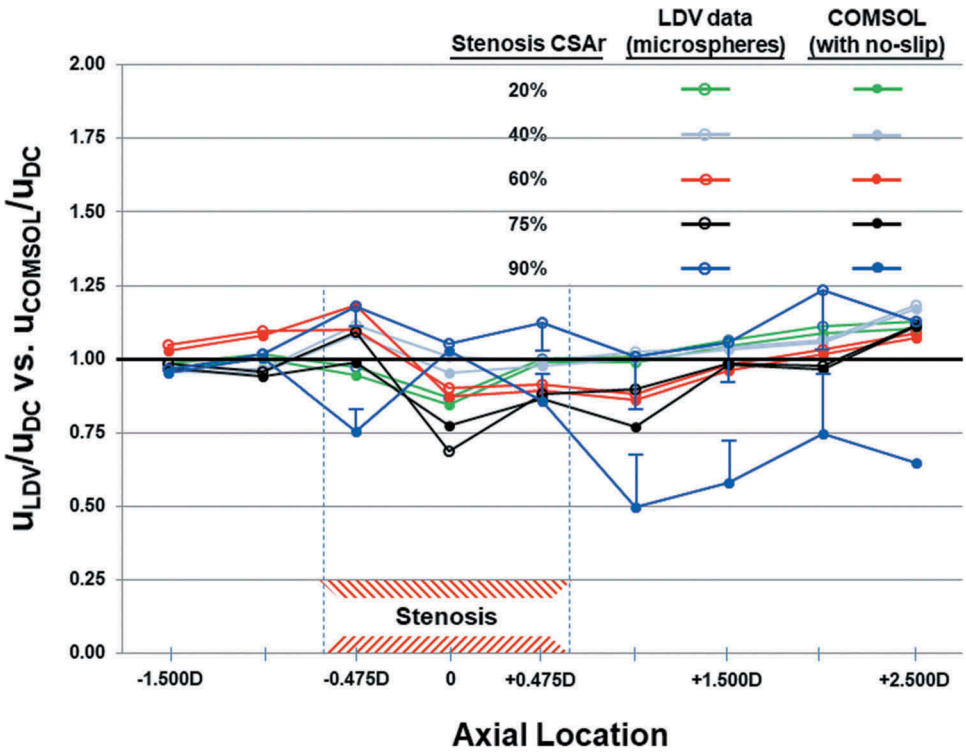

Figure 6. Ratio of mean velocity predicted by combining LDV-derived microsphere velocities with beam power distribution data to mean velocity recorded by scaled-up Doppler catheter (u_{LDV}/u_{DC} - open rings) vs. ratio of mean velocity predicted by combining COMSOL simulations with beam power distribution data to mean velocity recorded by scaled-up Doppler catheter (u_{COMSOL}/u_{DC} - closed rings). COMSOL simulation imposed no-slip condition at all surfaces. The beam power within the body of each stenosis was set to zero (in accordance with paraffin absorbing ultrasound), and beam expansion was included distal to each stenosis [24]. Error bars represent 1SD from the mean value and are shown where data differ by >2SD. LDV = laser Doppler velocimetry; DC = scaled-up Doppler catheter; SD = standard deviation; CSAr = cross-sectional area reduction; D = test section inside diameter.

The detailed analysis of LDV measurements and COMSOL simulations, when held in the context of the no-slip nature of all surfaces and the fluid used in our model for the LDV measurements, indicate that the principle cause of the microsphere slip involved increased fluid shear rates. The physical point of actual microsphere slip caused by increased shear was likely at the interface of the microsphere surface and an ultra-thin (0.1–10 μm) boundary layer of experimental fluid, due to microsphere lateral migration and depletion [17,27]. Relative to adjacent model surfaces, this would translate into an "effective" slip. Multiple interactive fluid dynamic factors including inertia, lift forces and local flow separation [3–6, 17,27,28] may have influenced migration, depletion and slip. Although we did not investigate the relative contributions of each factor in our model, together they may account for the increased slip velocity we observed at the central cylinder surface proximal to stenoses ([0.80 ± 0.21]×[mean velocity]) compared with experimental results involving concentrated suspensions ([0.1–0.4]×[mean velocity]) [5,6]. Also, our observed slip is similar to the deviation in microsphere velocity profile described by Uijttewaal, et al. [17], whose microsphere diameter and concentration were similar to ours.

The detailed analysis also showed that the critical threshold fluid shear rate for the development of microsphere slip was 10.61 cm^{-1} (normalized to mean velocity [in $cm \times sec^{-1}$]). This critical normalized threshold is only 3.38×the normalized shear rate at locations of no-slip and no other flow disturbance (specifically, adjacent to the test section surface at axial location −1.500; where normalized shear rate = 3.14 cm^{-1}). Thus, if the mean velocity of coronary blood flow down a proximal left anterior descending coronary artery was 30 $cm \times sec^{-1}$, then the critical threshold fluid shear rate would be only 318.3 sec^{-1}. However, in the absence of disease or inhibitory drugs, the adhesive macromolecules which mediate interactions between platelets and different surfaces in the development of thrombus *in-vivo* [14,29] likely limit the interruption in physical contact between the platelet and surfaces caused by their slip, and therefore likely drive up the critical normalized threshold fluid shear rate for platelet slip *in-vivo*. Additionally, although geometric surface roughness and hydrophilicity did not appreciably affect LDV-measured slip in our model, they may affect platelet slip *in-vivo* [30]. Finally, despite the fluid dynamic similarity between rigid microspheres and platelets [17], the unique discoid shape of platelets may affect their margination, collision and adhesion dynamics [31,32], and therefore may also contribute to an increase in the in-vivo critical normalized fluid shear rate.

The presence of platelet slip in the *in-vivo* setting, subtracting any effect of adhesive macromolecules, endothelial surface roughness and platelet discoid shape, would nonetheless diminish adhesion and thrombosis. This diminishment explains several important basic and clinical cardiovascular observations. For example, Sakariassen, et al. [33] studied platelet adhesion to subendothelium in an annular perfusion chamber–a geometry similar to our model with the central cylinder present–at RE 47–124. They found platelet adhesion at the central surface initially increased with increasing RE. However, the authors observed, "at the two highest flow rates tested (RE 98–124), the difference in platelet adhesion between the flow systems was slightly less." This observation would be consistent with the onset of platelet slip in the range RE 98–124.

Moreover, Strony, et al. [34] showed that, in a model of non-ruptured coronary artery stenosis (mean CSAr, 82 ± 8%), aggregation of platelets with the development of platelet-rich thrombi occurred ~0.4 vessel diameter distal to their stenosis entrance. This was attributed to shear-induced platelet activation at the

stenosis entrance [35] followed by adhesion and aggregation within the interior of the stenosis, "under the influence of a developing parabolic flow profile." [34] Our data suggest that, more precisely, the shear-induced activated platelets slipped at the stenosis entrance but that the slip progressively diminished distally to below a threshold where adhesive macromolecules dominated, thus accounting for adhesion and aggregation at the more distal site.

From a more clinical application perspective, thrombus formation on devices such as guide wires and catheters appears to be initiated by the coagulation system [36,37]. Moreover, the adhesion of flowing platelets at lower shear rates is mediated by fibrinogen and at higher shear rates somewhat more effectively by von Willebrand factor [38]. However, a comparison of different semi-quantitative studies of thrombus formation on devices shows that the quantity of thrombus formed paradoxically diminishes with increasing blood flow [36,39]. Our results suggest that the interaction of platelets with these device surfaces is diminished by slip while blood flows at RE typical of coronary flow. Therefore, any thrombotic consequence of activity of the coagulation system on these surfaces is diminished. Moreover, platelets may nonetheless become activated within and distal to stenoses and along these device surfaces due to plasma shear rate effects (via activated plasma von Willebrand factor and the platelet shear receptors, glycoproteins Ib/V/IX [40]). Also, any disordering of platelet shear rates distal to stenoses, indicating a disturbance in their flow, may independently cause their activation (via multiple mechanisms independent of von Willebrand factor-glycoproteins Ib/V/IX interactions [41]). From these perspectives, antiplatelet therapy would prove critical in limiting consequent thrombosis. Our results therefore provide a direct experimental fluid dynamic foundation for antiplatelet-focused antithrombotic therapy-without scheduled anticoagulation-during catheter-based coronary interventions directed towards higher grade atherosclerotic stenoses [42,43].

Limitations

Our model has several limitations: (1) platelets are biologic and geometrically biconvex discoid (in their inactive state) rather than inert and spherical; (2) it represents an idealized flow and geometric scenario; (3) no surface contained the macromolecules found in biologic systems; (4) the effect of microsphere rotation, although likely minor [44], was not addressed; and (5) interpolation of LDV data may have introduced small errors [16].

Conclusions

Our validated model establishes proof of concept for platelet slip. Additionally, platelet slip explains several important basic and clinical cardiovascular observations, and underscores that the topic deserves further exploration. If future technological advances allow confirmation of platelet slip in a true biologic environment-including surface proteins and receptors, and perhaps using lyophilized platelets-then our model will likely influence the development of shear-dependent antiplatelet (and other) drugs. Moreover, adding shear rate information, our model provides a direct experimental fluid dynamic foundation for antiplatelet-focused antithrombotic therapy during coronary interventions directed towards higher grade atherosclerotic stenoses. Finally, although the most immediate and important application of our model is to the platelet, the results may also apply and prove useful in other domains (e.g. cardiovascular, fluid dynamic, biomedical and mechanical engineering).

Acknowledgements

The authors wish to express appreciation to B. Pat Denardo (deceased) from the National Aeronautics and Space Administration Ames Research Center (Sunnyvale, CA) for critical advising in the design of the test section, and Professor Lawrence Talbot (deceased) from the College of Engineering at the University of California, Berkeley, for scientific and technical advising in other design aspects and data collection for this research project.

The authors also thank Professor Mark Walters, Director of the Duke University Shared Materials Instrumentation Facility (SMIF), for surface roughness measurements. SMIF is a member of the North Carolina Research Triangle Nanotechnology Network (RTNN), which is supported by the National Science Foundation (Grant ECCS-1542015) as part of the National Nanotechnology Coordinated Infrastructure (NNCI).

Funding

This work was supported by: American Heart Association [California Affiliate Grant 88-N7]; North Carolina Research Triangle Nanotechnology Network [Kickstarter Program].

Declaration of Interest

The authors report no conflicts of interest.

References

1. Navier CLMH. Memoire sur les lois du mouvement des fluides. Mem Acad R Sci Inst France 1823;6:389–440.
2. Lauga E, Brenner MP, Stone HA. Handbook of experimental fluid dynamics. New York: Springer; 2005, Chap. 15.
3. Van den Akker HEA. Mesoscale flow structures and fluid–particle interactions. Adv Chem Eng 2015;46:281–354. doi:10.1016/bs.ache.2015.10.010
4. Cloitre M, Bonnecaze RT. A review on wall slip in high solid dispersions. Rheol Acta 2017;56:283–305. doi:10.1007/s00397-017-1002-7
5. Koh CJ, Hookham P, Leal LG. An experimental investigation of concentrated suspension flows in a rectangular channel. J Fluid Mech 1994;266:1–32. doi:10.1017/S0022112094000911
6. Jesinghausen S, Weiffen R, Schmid H-J. Direct measurement of wall slip and slip layer thickness of non-Brownian hard-sphere suspensions in rectangular channel flows. Exp Fluids 2016;57:153–167. doi:10.1007/s00348-016-2241-6
7. Weddell JC, Kwack J, Imoukhuede PI, Masud A. Hemodynamic analysis in an idealized artery tree: differences in wall shear stress between Newtonian and non-Newtonian blood models. PLoS One 2015;10:e0124575. doi:10.1371/journal.pone.0124575
8. Mooney M. Explicit formulas for slip and fluidity. J Rheol 1931;2:210–222. doi:10.1122/1.2116364
9. Bennett L. Red cell slip at a wall in vitro. Science 1967;155:1554–1556. doi:10.1126/science.155.3769.1554
10. Hershey D, Cho SJ. Blood flow in rigid tubes: thickness and slip velocity of plasma film at the wall. J Appl Physiol 1966;1:27–32. doi:10.1152/jappl.1966.21.1.27
11. Coleman RW, Hirsh J, Marder VJ et al., editors. Hemostasis and thrombosis: basic principles and clinical practice, 4th ed. Philadelphia: Lippincott Williams and Wilkins; 2001, p. 575–596.
12. Sorrentino S, Studt JD, Medalia O, Tanuj Sapra K. Roll, adhere, spread and contract: structural mechanics of platelet function. Eur J Cell Biol 2015;94:129–138. doi:10.1016/j.ejcb.2015.01.001
13. Fasano A, Pavlova J, Sequeira A. A synthetic model for blood coagulation including blood slip at the vessel wall. Clin Hemorheol Microcirc 2013;54:1–14. doi:10.3233/CH-2012-1558
14. Mustard JF, Packham MA, Kinlough-Rathbone RL, Perry DW, Regoeczi E. Fibrinogen and ADP-induced platelet aggregation. Blood 1978;52:453–466. PMID:96891
15. Denardo SJ, Talbot L, Hargrave VK, Fitzgerald PJ, Selfridge AR, Yock PG. Analysis of pulsed wave Doppler ultrasound spectra obtained from a model intracoronary catheter. IEEE Trans Biomed Eng 1994;41:635–648. doi:10.1109/10.301730
16. Ahmed SA, Giddens DP. Velocity measurements in steady flow through axisymmetric stenoses at moderate Reynolds numbers. J Biomech 1983;16:505–516. doi:10.1016/0021-9290(83)90065-9

17. Uijttewaal WS, Nijhof EJ, Heethaar RM. Lateral migration of blood cells and microspheres in two-dimensional Poiseuille flow: a laser-Doppler study. J Biomech 1994;27:35–42. doi:10.1016/0021-9290(94)90030-2
18. Tabor D, Winterton RHS. The direct measurement of normal and retarded van der Waals forces. Proc Roy Soc A 1969;312:435–450. doi:10.1098/rspa.1969.0169
19. Kajiya F, Tomonaga G, Tsujioka K, Ogasawara Y, Nishihara H. Evaluation of local blood flow velocity in proximal and distal coronary arteries by laser Doppler method. J Biomech Eng 1985;107:10–15. doi:10.1115/1.3138511
20. Boyce JF, Wong PC, Schürch S, Roach MR. Rabbit arterial endothelium and subendothelium. A change in interfacial free energy that may promote initial platelet adhesion. Circ Res 1983;53:372–377. doi:10.1161/01.res.53.3.372
21. Burton HE, Freij JM, Espino DM. Dynamic viscoelasticity and surface properties of porcine left anterior descending coronary arteries. Cardiovasc Eng Technol 2017;8:41–56. doi:10.1007/s13239-016-0288-4
22. Durst F, Muller R. Determination of the measuring position in laser-Doppler anemometry. Exp Fluids 1988;6:105–110. doi:10.1007/BF00196460
23. Armaly BF, Durst F, Pereira JCF, Schönung B. Experimental and theoretical investigation of backward-facing step flow. J Fluid Mech 1983;127:473–496. doi:10.1017/S0022112083002839
24. Dietz DR, Parks SI, Linzer M. Expanding-aperture annular array. Ultrason Imaging 1979;1:56–75. doi:10.1177/016173467900100105.
25. Denardo SJ, Yamada EG, Hargrave VK, Yock PG. Effect of stenosis inlet geometry on shear rates of blood flow in the upstream region. Am Heart J 1993;125:350–356. doi:10.1016/0002-8703(93)90011-w
26. Lande R. On comparing coefficients of variation. Syst Zool 1977;26:214–217. doi:10.2307/2412845
27. Barnes HA. A review of the slip (wall depletion) of polymer solutions, emulsions and particle suspensions in viscometers: its cause, character, and cure. J Non-Newtonian Fluid Mech 1995;56:221–251. doi:10.1016/0377-0257(94)01282-M
28. Sherry M, Lo Jacono D, Sheridan J. An experimental investigation of the recirculation zone formed downstream of a forward facing step. J Wind Eng Ind Aerodyn 2010;98:888–894. doi:10.1016/j.jweia.2010.09.003
29. Chang KC, Hammer DA. The forward rate of binding of surface-tethered reactants: effect of relative motion between two surfaces. Biophys J 1999;76:1280–1292. doi:10.1016/S0006-3495(99)77291-7
30. Zingg W, Neumann AW, Strong AB, Hum OS, Absolom DR. Effect of surface roughness on platelet adhesion under static and under flow conditions. Can J Surg 1982;25:16–19. PMID:7055757
31. Gentile F, Chiappini C, Fine D, Bhavane RC, Peluccio MS, Cheng MM, Liu X, Ferrari M, Decuzzi P. The effect of shape on the margination dynamics of non-neutrally buoyant particles in two-dimensional shear flows. J Biomech 2008;41:2312–2318. doi:10.1016/j.jbiomech.2008.03.021
32. Mody NA, King MR. Platelet adhesive dynamics. Part I: characterization of platelet hydrodynamic collisions and wall effects. Biophys J 2008;95:2539–2555. doi:10.1529/biophysj.107.127670
33. Sakariassen KS, Bolhuis PA, Sixma JJ. Platelet adherence to subendothelium of human arteries in pulsatile and steady flow. Thromb Res 1980;19:547–559. PMID:6969464
34. Strony J, Beaudoin A, Brands D, Adelman B. Analysis of shear stress and hemodynamic factors in a model of coronary artery stenosis and thrombosis. Am J Physiol 1993;265(5 Pt 2):H1787–H1796. doi:10.1152/ajpheart.1993.265.5.H1787.
35. Badimon L, Chesebro JH, Badimon JJ. Thrombus formation on ruptured atherosclerotic plaques and rethrombosis on evolving thrombi. Circulation 1992;86(6Suppl):III74–85. PMID:1424053
36. Aldenhoff YB, Hanssen JH, Knetsch ML, Koole LH. Thrombus formation at the surface of guide-wire models: effects of heparin-releasing or heparin-exposing surface coatings. J Vasc Interv Radiol 2007;18:419–425. doi:10.1016/j.jvir.2006.12.733
37. Yau JW, Stafford AR, Liao P, Fredenburgh JC, Roberts R, Weitz JI. Mechanism of catheter thrombosis: comparison of the antithrombotic activities of fondaparinux, enoxaparin, and heparin in vitro and in vivo. Blood 2011;118:6667–6674. doi:10.1182/blood-2011-07-364141
38. Savage B, Saldívar E, Ruggeri ZM. Initiation of platelet adhesion by arrest onto fibrinogen or translocation on von Willebrand factor. Cell 1996;84:289–297. doi:10.1016/s0092-8674(00)80983-6
39. Gobeil F, Juneau C, Plante S. Thrombus formation on guide wires during routine PTCA procedures: a scanning electron microscopic evaluation. Can J Cardiol 2002;18:263–269. PMID:11907615
40. Chow TW, Hellums JD, Moake JL, Kroll MH. Shear stress-induced von Willebrand factor binding to platelet glycoprotein Ib initiates calcium influx associated with aggregation. Blood 1992;80:113–120. PMID:1611079
41. Slepian MJ, Sheriff J, Hutchinson M, Tran P, Bajaj N, Garcia JGN, Scott Saavedra S, Bluestein D. Shear-mediated platelet activation in the free flow: perspectives on the emerging spectrum of cell mechanobiological mechanisms mediating cardiovascular implant thrombosis. J Biomech 2017;50:20–25. doi:10.1016/j.jbiomech.2016.11.016
42. Stabile E, Nammas W, Salemme L, Sorropago G, Cioppa A, Tesorio T, Ambrosini V, Campopiano E, Popusoi G, Biondi Zoccai G, et al. (Coronary Interventions Antiplatelet-based Only) Study: a randomized study comparing standard anticoagulation regimen to absence of anticoagulation for elective percutaneous coronary intervention. J Am Coll Cardiol 2008;52:1293–1298. doi:10.1016/j.jacc.2008.07.026
43. Denardo SJ, Davis KE, Tcheng JE. Effectiveness and safety of reduced-dose enoxaparin in non-ST-segment elevation acute coronary syndrome followed by antiplatelet therapy alone for percutaneous coronary intervention. Am J Cardiol 2007;100:1376–1382. doi:10.1016/j.amjcard.2007.06.024
44. Leach J, Mushfique H, Keen S, Di Leonardo R, Ruocco G, Cooper JM, Padgett MJ. Comparison of Faxen's correction for a microsphere translating or rotating near a surface. Phys Rev E 2009;79:026301–1–4. doi:10.1103/PhysRevE.79.026301